

# Delayed or absent $\pi(h_{11/2})^2$ alignment in $^{111}\text{Xe}$

L. Capponi,<sup>1,2,3</sup> J. F. Smith,<sup>1,2,\*</sup> P. Ruotsalainen,<sup>4</sup> C. Scholey,<sup>4</sup> P. Rahkila,<sup>4</sup> L. Bianco,<sup>5</sup>  
A. J. Boston,<sup>6</sup> H. C. Boston,<sup>6</sup> D. M. Cullen,<sup>7</sup> X. Derkx,<sup>1,2</sup> M. C. Drummond,<sup>6</sup> T. Grahn,<sup>4</sup>  
P. T. Greenlees,<sup>4</sup> L. Grocutt,<sup>1,2</sup> B. Hadinia,<sup>5</sup> U. Jakobsson,<sup>4,†</sup> D. T. Joss,<sup>6</sup> R. Julin,<sup>4</sup>  
S. Juutinen,<sup>4</sup> M. Labiche,<sup>8</sup> M. Leino,<sup>4</sup> K. G. Leach,<sup>5,‡</sup> C. McPeake,<sup>6</sup> K. F. Mulholland,<sup>1,4</sup>  
P. Nieminen,<sup>4</sup> D. O'Donnell,<sup>1,2</sup> E. S. Paul,<sup>6</sup> P. Peura,<sup>4,§</sup> M. Sandzelius,<sup>4</sup> J. Sarén,<sup>4</sup>  
B. Saygi,<sup>6,¶</sup> J. Sorri,<sup>4,\*\*</sup> S. Stolze,<sup>4,††</sup> A. Thornthwaite,<sup>6</sup> M. J. Taylor,<sup>7,‡‡</sup> and J. Uusitalo<sup>4</sup>

<sup>1</sup>*School of Computing, Engineering, and Physical Sciences,  
University of the West of Scotland,  
Paisley, PA1 2BE, United Kingdom*

<sup>2</sup>*Scottish Universities Physics Alliance*

<sup>3</sup>*ELI-NP, Horia Hulubei National Institute of Physics  
and Nuclear Engineering, 077125 Magurele, Romania*

<sup>4</sup>*University of Jyväskylä, Department of Physics,  
P.O. Box 35, FIN-40014 University of Jyväskylä, Finland*

<sup>5</sup>*Department of Physics, University of Guelph,  
Guelph, Ontario, N1G 2W1, Canada*

<sup>6</sup>*Oliver Lodge Laboratory, University of Liverpool,  
Liverpool, L69 7ZE, United Kingdom*

<sup>7</sup>*School of Physics and Astronomy,  
Schuster Laboratory, University of Manchester,  
Manchester, M13 9PL, United Kingdom*

<sup>8</sup>*Nuclear Physics Group, STFC Daresbury Laboratory,  
Daresbury, Warrington, WA4 4AD, United Kingdom*

(Dated: October 31, 2019)

# Abstract

Accepted for publication in Phys. Rev. C on 31st October 2019

Excited states have been identified in the very neutron-deficient  $N = Z + 3$  nucleus  $^{111}\text{Xe}$  for the first time, using the  $^{58}\text{Ni}(^{58}\text{Ni},\alpha n)$  heavy-ion fusion-evaporation reaction. Gamma-ray transitions have been unambiguously assigned to  $^{111}\text{Xe}$  by correlation with the characteristic  $^{111}\text{Xe} \rightarrow ^{107}\text{Te} \rightarrow ^{103}\text{Sn}$   $\alpha$ -decay chain using the method of recoil-decay tagging. Inspection of  $\gamma\gamma$  coincidence data has shown that five of the transitions form a rotational-like sequence. Excitation-energy systematics suggest that the sequence could be the favored signature partner of a band built on an  $h_{11/2}$  neutron. Aligned angular momenta of states in the band have been compared to analogous bands in neighboring xenon isotopes. The aligned angular momenta for the  $^{111}\text{Xe}$  band are constant over the range of observed rotational frequencies, suggesting that the first  $\pi(h_{11/2})^2$  alignment is either delayed or absent. It is speculated that the alignment of  $h_{11/2}$  protons in the presence of neutrons in near-identical  $h_{11/2}$  orbitals may be affected by neutron-proton interactions, or by the onset of octupole correlations.

PACS numbers: 23.20.Lv, 23.60.+e, 27.60.+j, 29.30.Kv

---

\*Electronic address: [John.F.Smith@uws.ac.uk](mailto:John.F.Smith@uws.ac.uk)

†Present address: Laboratory of Radiochemistry, Department of Chemistry, University of Helsinki, P.O. Box 55, FIN-00014 Helsinki, Finland

‡Present address: Department of Physics, Colorado School of Mines, Golden Colorado 80401, USA

§Present address: Helsinki Institute of Physics, P.O.Box 64, FI-00014 University of Helsinki, Finland

¶Present address: Department of Physics, Ege Üniversitesi, Bornova, İzmir, Turkey

\*\*Present address: Sodankylä Geophysical Observatory, University of Oulu, 90014 Oulu, Finland

††Present address: Argonne National Laboratory, Physics Division, Lemont, IL 60439, USA

‡‡Present address: Division of Cancer Sciences, School of Medical Sciences, University of Manchester, Manchester, M13 9PL, UK

**CORRESPONDING AUTHOR:**

Professor John F. Smith

**Address:**

School of Computing, Engineering, and Physical Sciences,  
University of the West of Scotland,  
Paisley Campus,  
Paisley,  
PA1 2BE  
Scotland UK

**Tel:** 44 141 848 3652

**Fax:** 44 141 848 3404

**Email:** John.F.Smith@uws.ac.uk

## I. INTRODUCTION

One of the main drivers in contemporary nuclear-structure physics is the quest to achieve a better understanding of the nature of nuclei far from stability (for example, [1]). In this context, the very neutron-deficient nuclei just above the  $N = Z = 50$  closed shells are of particular interest. This region contains the heaviest self-conjugate nuclei that are expected to have bound excited states, and with realistic prospects of experimental study. Near  $N = Z$ , neutrons and protons will occupy near-identical orbitals giving a large spatial overlap in their wave functions, and an increased likelihood of neutron-proton ( $np$ ) correlations. This is especially interesting in nuclei with several valence nucleons of each type, where single-particle excitations start to give way to the development of collectivity. Just above  $N = Z = 50$ , the orbitals near the Fermi levels will emanate from the  $d_{5/2}$ ,  $g_{7/2}$ , and  $h_{11/2}$  subshells. The  $d_{5/2}$  and  $h_{11/2}$  subshells have  $\Delta\ell = \Delta j = 3$ , so the simultaneous occupation of orbitals from these subshells has led to the expectation that octupole correlations will become important [2, 3]. Calculations [3] suggest that octupole correlations in this region are maximized for  $N = Z = 56$  ( $^{112}\text{Ba}$ ), but that they will also play an important role in neighboring nuclei. Furthermore, in this region, the octupole-driving orbitals are the same orbitals for both neutrons and protons leading to the possibility of octupole correlations *between* the neutrons and protons.

For the light  $Z = 54$  xenon isotopes, ground-state deformations were compiled and systematically studied by Raman *et al.*, in Ref. [4]. That work focussed on the relationship between the excitation energies of the  $2_1^+$  states and the measured  $B(E2; 0_1^+ \rightarrow 2_1^+)$  values in the even-even nuclei. Experimental data compiled in Ref. [5] suggest that the ground-state deformation is largest for the  $N = 66$  neutron-midshell nucleus  $^{120}\text{Xe}$ , and that the deformation decreases with decreasing  $N$ . However, it was noted in Ref. [5] that the deformation of the  $N = 58$  nucleus  $^{112}\text{Xe}$  is larger than would be expected from the established systematic trend. A similar “larger than expected” deformation was also later inferred for the  $N = 56$  nucleus  $^{110}\text{Xe}$  [6]. The behavior of the ground-state deformation with decreasing  $N$  is not understood, but it is suggested in Ref. [6] that isoscalar  $np$  interactions may play a part. In  $N = 58$   $^{112}\text{Xe}$  [5] the observation of a low-lying negative-parity band linked to the ground-state band by enhanced E1 transitions has been taken as tentative evidence for the onset of octupole correlations. The development of octupole correlations may influence the behavior

of the inferred ground-state deformations.

From an experimental perspective, valuable structural information can be extracted from the identification of just a few excited states. To this end,  $\gamma$ -ray spectroscopy is a very useful technique. However, experiments to study the nuclei with  $N \simeq Z$  and  $A \simeq 110$  are challenging. The best way to produce these nuclei is to use heavy-ion fusion-evaporation reactions with the most neutron-deficient stable beams and targets available. The most neutron-deficient evaporation residues are produced by neutron evaporation but the cross-sections for neutron evaporation from already neutron-deficient compound nuclei are very small. Consequently, the nuclei of interest are produced together with a large number of more intense products. In order to study the most neutron-deficient nuclei in  $\gamma$ -ray spectroscopy experiments, highly selective methods of channel selection and identification are needed. As such, the method of recoil-decay tagging (RDT) [7, 8] has become established, which enables the  $\gamma$ -ray spectroscopy of nuclei that have a characteristic ground-state decay such as  $\alpha$ -particle or proton emission. The RDT method involves the detection of prompt  $\gamma$  rays at the reaction site followed by detection of the arrival and characteristic decay of evaporation residues at the focal plane of a recoil separator. In this way, prompt  $\gamma$  rays can be correlated with evaporation residues that have characteristic decay properties, giving unambiguous identification of the nucleus that emitted the  $\gamma$  rays. The lightest xenon isotopes that have been identified,  $^{108,109,110,111}\text{Xe}$ , are known to have ground states that decay by  $\alpha$ -particle emission. Excited states have already been identified in  $^{110}\text{Xe}$  using the RDT method [6]. Prior to the present work, there were no known excited states in the nucleus  $^{111}\text{Xe}$ .

## II. PREVIOUS STUDIES OF ODD-A XENON ISOTOPES

The lightest stable  $Z = 54$  xenon isotope is  $^{124}\text{Xe}$  ( $N = 70$ ) and the lightest xenon isotope that has been experimentally identified is  $^{108}\text{Xe}$  ( $N = Z = 54$ ) [9]. The xenon isotopes with  $N \leq 59$  are known to decay by  $\alpha$  particle emission, with increasingly large  $\alpha$ -decay branches ( $b_\alpha$ ) as  $N$  decreases. The isotopes  $^{113,112}\text{Xe}$  have  $b_\alpha < 1\%$  [10, 11], whereas the  $b_\alpha$  values are  $\sim 10\%$  [10, 12],  $\sim 65\%$  [13], and  $100\%$  [14] for  $^{111,110,109}\text{Xe}$ , respectively. Alpha decay of the  $N = Z$  nucleus  $^{108}\text{Xe}$  was reported recently in Ref. [9]; in that work, it is assumed that  $b_\alpha = 100\%$  although only two  $\alpha$ -decay events are observed. Of particular interest in the present work is the  $\alpha$  decay of  $^{111}\text{Xe}$  and that of its daughter  $^{107}\text{Te}$ . The  $\alpha$  decays of

these nuclei were first reported by Schardt *et al.* in Ref. [10]. The decays of these nuclei were subsequently studied again as reported in Refs. [11, 12, 16, 17]. For  $^{111}\text{Xe}$ , two  $\alpha$  decays have been reported with  $E_\alpha = 3580(30)$  keV and  $3480(15)$  keV [16] and  $b_\alpha = 8(2)\%$  and  $3(2)\%$  [12], respectively. Both decays have  $T_{1/2} \simeq 900(200)$  ms [10] suggesting that they originate from the same state. The  $\alpha$  decay of  $^{107}\text{Te}$  has been reported with  $E_\alpha = 3862(10)$  keV [17],  $b_\alpha = 70(30)\%$  [10] and  $T_{1/2} = 3.1(0.1)$  ms [11].

To date, excited states have been identified in all of the neutron-deficient xenon isotopes down to  $^{110}\text{Xe}$  ( $N = 56$ ) with the exception of  $^{111}\text{Xe}$  ( $N = 57$ ). The isotopes  $^{114-122}\text{Xe}$  ( $60 \leq N \leq 68$ ) can be produced with relatively large cross sections in heavy-ion fusion evaporation reactions, and consequently have been well studied in  $\gamma$ -ray spectroscopy experiments, with multiple high-spin rotational bands being observed in many of these nuclei (for example, in Refs. [18–28]). For  $N < 60$ , the xenon isotopes can only be produced in fusion-evaporation reaction channels that involve neutron evaporation, and consequently the cross sections become increasingly small as  $N$  decreases. The nuclei  $^{113,112}\text{Xe}$  have been studied by detecting evaporated charged particles and neutrons as a means of channel selection using the “Microball method” [29, 30]. In  $^{113}\text{Xe}$ , produced in the  $^{58}\text{Ni}(^{58}\text{Ni}, 2pn)$  reaction, eight rotational bands were observed, with a maximum spin of  $30 \hbar$  [31] above the ground state. In  $^{112}\text{Xe}$ , produced in the  $^{58}\text{Ni}(^{58}\text{Ni}, 2p2n)$  reaction, two rotational bands were observed up to  $\sim 12 \hbar$  [5]. For  $N < 58$ , the production cross sections are too small ( $< 1 \mu b$ ) to use the detection of evaporated particles for channel selection. However, because the ground states of these nuclei decay by  $\alpha$ -particle emission, they can be studied by the method of recoil-decay tagging (RDT) [8]. Indeed, excited states have already been identified in the nucleus  $^{110}\text{Xe}$ , using the  $^{58}\text{Ni}(^{54}\text{Fe}, 2n)$  reaction, despite the very small cross section of 50 nb [6]. In the present work, excited states have been identified in  $^{111}\text{Xe}$  for the first time, using the RDT method with the  $^{58}\text{Ni}(^{58}\text{Ni}, \alpha n)$  heavy-ion fusion-evaporation reaction; 15  $\gamma$ -ray transitions have been assigned to  $^{111}\text{Xe}$ , five of which are tentatively assigned to form the yrast  $\nu h_{11/2}$  band.

### III. EXPERIMENTAL DETAILS

In this work, results are presented from an experiment that was carried out using the K130 cyclotron at the Accelerator Laboratory of the University of Jyväskylä. The experiment

was designed to study the  $\alpha$  decay of the ground state of  $^{111}\text{Xe}$  as well as the  $\gamma$ -ray decay of its excited states. A beam of  $^{58}\text{Ni}$  ions, with energy 210 MeV, was incident upon a  $500\text{-}\mu\text{gcm}^{-2}$   $^{58}\text{Ni}$  target. Prompt  $\gamma$  rays, emitted at the reaction site, were detected using the Jurogam-II  $\gamma$ -ray spectrometer [32] consisting of 15 coaxial HPGe detectors and 24 Clover HPGe detectors. Recoiling reaction products were separated from the primary and scattered beam by the RITU gas-filled recoil separator [33]. At the focal plane of RITU, the reaction products passed through a multi-wire proportional counter (MWPC) before being implanted into one of two adjacent double-sided silicon strip detectors (DSSDs) each of thickness  $300\text{ }\mu\text{m}$  and with 40 horizontal (front) strips and 60 vertical (back) strips, giving a total of 4800 DSSD pixels. A planar HPGe detector was placed 3 mm behind the DSSDs and three Clover HPGe detectors were placed around the DSSDs; relative to the center of the DSSDs, the centers of the Clover detectors had polar coordinates  $(\theta, \phi)$  of  $(90^\circ, 0^\circ)$ ,  $(90^\circ, 90^\circ)$  and  $(90^\circ, 270^\circ)$ , where  $\theta = 0^\circ$  is the central ion trajectory and  $\phi = 0^\circ$  is vertically upwards. The MWPC, DSSDs, planar HPGe, and (focal-plane) Clover HPGe detectors are part of the GREAT spectrometer [34]. The Total Data Readout (TDR) data-acquisition system was used [35] in which a 100-MHz clock provided a timestamp on each detector signal; thus, the time of each detector signal was recorded to the nearest 10 ns. Data were recorded for all detector signals received within a fixed time window around either (a) a signal in the DSSDs (implantation of a nucleus or decay of an implanted nucleus) or (b)  $\geq 2$  prompt signals in the Jurogam-II spectrometer. The beam intensity was limited to an average value of 2 pA for the duration of the experiment in order to keep the implantation rate in the DSSD appropriate for implant-decay correlations of  $^{111}\text{Xe}$  ( $T_{1/2} \simeq 900\text{ ms}$ ). The experimental details and apparatus used are described in detail in Ref. [36].

During the experiment, detector signals and their timestamps were recorded to hard disk. In total,  $\sim 1$  TB of data were collected. The data were analysed using the GRAIN [37] and RADWARE [38, 39] software packages. The HPGe detectors, in Jurogam-II and at the focal plane of RITU, were calibrated using standard calibration sources of  $^{152}\text{Eu}$  and  $^{133}\text{Ba}$ . The DSSDs were initially gain-matched using a mixed source of  $^{239}\text{Pu}$ ,  $^{241}\text{Am}$ , and  $^{244}\text{Cm}$ , which emit  $\alpha$  particles with energies in the range of 5 to 6 MeV. In addition, an internal calibration of the DSSDs was performed using the  $^{58}\text{Ni}$  beam, with energy 235 MeV, incident on a natural molybdenum target; the known energies of protons and  $\alpha$  particles emitted by the proton-rich  $^{66}\text{Dy}$ ,  $^{68}\text{Er}$ , and  $^{70}\text{Yb}$  nuclei implanted into the DSSD were then used to

calibrate the individual DSSD strips.

#### IV. DATA ANALYSIS AND RESULTS

The RDT method was used to search for  $\gamma$ -ray transitions from excited states of  $^{111}\text{Xe}$ . The method involved the following steps: (i) detection of prompt  $\gamma$  rays at the reaction site (at time  $t_\gamma$ ); (ii) detection of the implantation of the evaporation residue into one pixel of the DSSDs at the focal plane of RITU (at time  $t_{\text{implant}}$ ); and (iii) measurement of the decay of the implanted residue in the same pixel (at time  $t_{\text{decay}}$ ). In this way, prompt  $\gamma$  rays were correlated in time with implanted nuclei, and the implanted nuclei were correlated in space to the observation of characteristic decays, giving unambiguous identification of the nucleus that emitted the  $\gamma$  rays. A signal in the DSSDs can correspond to the implantation of a nucleus or to the decay of a previously implanted nucleus. Therefore an important first step in the data analysis is to distinguish between these two cases: implantation events were defined by a time correlation with a signal from the MWPC (with no DSSD energy constraint) or a DSSD energy  $\geq 7$  MeV, whereas decay events were defined as those with no time-correlated MWPC signal and with DSSD energy  $< 7$  MeV. Ultimately, this process resulted in  $9 \times 10^8$  implantation events (henceforth called *implants*) and  $2 \times 10^7$  decay events (*decays*) in the DSSDs. Subsequent to the broad definition of decays, the decays of specific nuclei were selected using the measured decay energies and decay times. The maximum time interval between the implant and decay ( $t_{\text{decay}} - t_{\text{implant}}$ ) [or between the decay of an implant and the subsequent decay of its daughter ( $t_{\text{decay}2} - t_{\text{decay}1}$ )] is called the *search time*; this was constrained to match the nucleus of interest. Often a search time of  $3 \times T_{1/2}$  is used, within which almost 90% of the nuclei of interest will decay. A requirement on the decay energy can also be used, but because  $\alpha$  particles can escape from the DSSD after only partially depositing their energies, the accepted energy range needs to be carefully considered.

Initially, the  $\alpha$ -particle energy spectra from the DSSD were studied in order to identify peaks corresponding to  $\alpha$  decays of interest. An  $\alpha$ -particle energy spectrum was incremented with a search time of 6 s [ $\sim 7 \times T_{1/2}(^{111}\text{Xe})$ ] in order to identify  $\alpha$  particles emitted from  $^{111}\text{Xe}$ . Although peaks corresponding to the reported energies of the  $^{111}\text{Xe}$   $\alpha$  particles were apparent in the spectrum, they were superimposed on a large background, along with many other peaks. To improve the selectivity, it was required that following the first  $\alpha$  particle,



corresponding to the decay of  $^{111}\text{Xe}$ , a second  $\alpha$  particle, corresponding to the decay of the daughter nucleus  $^{107}\text{Te}$ , was observed. A search time of 12 ms [ $\sim 4 \times T_{1/2}(^{107}\text{Te})$ ] was used between the two  $\alpha$  particles. Using these conditions, a two-dimensional  $\alpha\alpha$  correlation matrix was incremented. The projections of this matrix are shown in Fig. 1; both projections show clear peaks, which illustrates the excellent selectivity provided by the requirement of the short-lived  $^{107}\text{Te}$   $\alpha$  decay. Figure 1(a) shows the energy of the first  $\alpha$  decay; peaks are observed with energies of 3474(16) and 3562(16) keV which are consistent with  $\alpha$  particles emitted from  $^{111}\text{Xe}$  [16]. Figure 1(b) shows the energy of the second  $\alpha$  decay; a peak is observed at 3851(17) keV, consistent with the  $\alpha$  particles emitted from  $^{107}\text{Te}$  [16]. In total,  $\sim 1300$   $^{111}\text{Xe}$  recoils were identified using the implant- $\alpha(^{111}\text{Xe})$ - $\alpha(^{107}\text{Te})$  correlation. The details of the  $\alpha$  decay of  $^{111}\text{Xe}$  as measured in the present work are not presented here but are discussed separately in Refs. [36, 40].

In order to correlate prompt  $\gamma$  rays with an implant, the condition  $80 \text{ ns} \leq (t_{\text{implant}} - t_{\gamma}) \leq 400 \text{ ns}$  was applied. The spectrum of prompt  $\gamma$  rays recorded with this condition is shown in Fig. 2(a). The main peaks in this spectrum can be attributed to known transitions in the most intensely-populated evaporation residues: some peaks corresponding to transitions in  $^{113}\text{I}$  ( $3p$  evaporation),  $^{114}\text{Xe}$  ( $2p$ ), and  $^{112}\text{Te}$  ( $4p$ ) are labelled. In order to search for  $\gamma$ -ray transitions from excited states in  $^{111}\text{Xe}$ , the RDT method was applied using the implant- $\alpha(^{111}\text{Xe})$ - $\alpha(^{107}\text{Te})$  correlation with search times of 6 s and 12 ms, as discussed above. In addition, it was required that the energies of the  $\alpha$  particles were in the range  $2 \leq E_{\alpha} \leq 7$  MeV; this broad gate was used to include  $\alpha$  particles that escaped from the DSSDs. The  $\gamma$ -ray spectra resulting from the RDT analysis are shown in Figs. 2(b), (c), and (d); all of the peaks labeled in these spectra have been assigned to  $^{111}\text{Xe}$ . Panel (b) shows the RDT-gated  $\gamma$ -ray (singles) spectrum, and Panel (c) shows the total projection of an RDT-gated  $\gamma\gamma$  correlation matrix. Panel (d) shows a coincidence spectrum gated on the 405-, 619-, or 783-keV transitions in the RDT-gated  $\gamma\gamma$  matrix. The stringent implant- $\alpha(^{111}\text{Xe})$ - $\alpha(^{107}\text{Te})$  condition was necessary to identify the  $\gamma$ -ray transitions belonging to  $^{111}\text{Xe}$ . Attempts were made to relax this condition to implant- $\alpha(^{111}\text{Xe})$  only, in order to increase the numbers of counts in the spectra. However, it was found that this relaxed condition was not sufficiently selective to allow observation of the  $^{111}\text{Xe}$   $\gamma$  rays.

From the RDT-gated spectra (Fig. 2), 15  $\gamma$ -ray transitions have been assigned to  $^{111}\text{Xe}$ . The transitions have energies up to  $\sim 1$  MeV, with the majority in the range from 400 to

800 keV; the energies and intensities of the transitions are listed in Tab. I. It is clear that there are differences in relative intensities of the transitions in the  $\gamma$ -ray singles spectrum [Fig. 2(b)] compared to the  $\gamma\gamma$  coincidence spectrum [Fig. 2(c)] which suggests that there are several different decay paths in  $^{111}\text{Xe}$  with different  $\gamma$ -ray multiplicities. In an attempt to determine the decay paths, and hence construct a level scheme, gates were set on the recoil-gated  $\gamma\gamma$  matrix. The spectrum of Fig. 2(d) shows the  $\gamma$  rays that are in coincidence with any of the 405-, 619-, or 783-keV  $\gamma$  rays. Although there are very few counts in this spectrum, peaks are apparent consisting of several clusters of counts on a background which is close to zero. This spectrum suggests the  $^{111}\text{Xe}$  level scheme has a sequence of coincident transitions with energies 405, 619, 783, 920, and 1048 keV. It was not possible to determine coincidence relationships for the remaining 10 transitions assigned to  $^{111}\text{Xe}$ .

## V. DISCUSSION

The sequence of coincident transitions assigned to  $^{111}\text{Xe}$  is shown in Fig. 3. The transitions have been ordered according to their relative intensities. The sequence is shown in comparison to the lowest six members of the yrast  $\nu h_{11/2}$  bands of the neutron-deficient odd- $A$  xenon isotopes  $^{113,115,117,119,121}\text{Xe}$  [19, 22, 23, 26, 31]. In the figure, the excitation energies of states in the bands are given relative to the respective  $11/2^-$  band heads. It is known from theoretical calculations (for example, [42]) and experimental studies of the neighboring nuclei that in  $\nu h_{11/2}$  configurations, these nuclei are reasonably well deformed, with  $\beta_2 \simeq 0.2$ . It is therefore expected that the excitation energies of states within the bands will vary smoothly as a function of neutron number  $N$ . It can be seen from Fig. 3 that as  $N$  decreases below  $^{121}\text{Xe}$  ( $N = 67$ ), there is good systematic agreement of the excitation energies, down to  $N = 59$  ( $^{113}\text{Xe}$ ). Furthermore, the new data for  $N = 57$  ( $^{111}\text{Xe}$ ) appear to agree reasonably well with the systematics. Some qualitative observations about the deformations of the  $\nu h_{11/2}$  configurations can be made by considering the spacings of the states within the bands. Below  $N = 67$ , the energy of the  $15/2^- \rightarrow 11/2^-$  transition decreases with decreasing  $N$  until  $N = 63$  ( $^{117}\text{Xe}$ ) where it reaches a minimum, beyond which it increases again for  $N = 61$  ( $^{115}\text{Xe}$ ). The transition has the same energy at  $N = 59$  ( $^{113}\text{Xe}$ ) as for  $N = 61$  implying that the deformation is constant for these two nuclei. For  $N = 57$  ( $^{111}\text{Xe}$ ) the energy is lower than for  $N = 59$  implying that the deformation increases again

as  $N$  is further reduced. This observation is interesting in the context of the neighboring  $^{110,112}\text{Xe}$  nuclei [5, 6] where the energies of the  $2_1^+$  and  $4_1^+$  states suggest that the deformation does not reduce as much as expected from the established systematic trend when moving towards  $N = 50$ . In Ref. [6] it is noted that there is a slight increase in  $B(E2; 2^+ \rightarrow 0^+)$  when going from  $^{112}\text{Xe}$  to  $^{110}\text{Xe}$ . The data on the far left of Fig. 3 show the excitation energies taken from shell-model calculations performed by Nowacki *et al.* [43]. The calculations were performed in the  $g_{7/2}, d_{5/2}, d_{3/2}, s_{1/2}, h_{11/2}$  valence space for neutrons and protons with a restriction of a maximum of five particles in the  $h_{11/2}$  subshells for each type of nucleon. The agreement between the excitation energies of the calculated and observed states is good with a difference of less than 200 keV for all of the states observed. This agreement supports the spin and parity assignments that were made from a consideration of excitation-energy systematics.

The assignment of the  $\nu h_{11/2}$  configuration to the  $^{111}\text{Xe}$  band can be further investigated by studying the aligned angular momenta of states in the band. Comparison of the experimental aligned angular momenta with theoretical predictions, together with the use of blocking arguments, can provide information about assignments underlying such rotational bands. In the present work, theoretical predictions were made using a procedure in which, as a first step, Total-Routhian Surface (TRS) calculations [44, 45] were carried out to determine the deformations in the lowest-lying configurations of the odd neutron. The deformations from the TRS calculations were subsequently used in Woods-Saxon cranked-shell-model (CSM) calculations [46] to calculate properties of the quasiparticle alignments, such as alignment frequencies, alignment gains, and interaction strengths, which were compared to the experimental observations.

The deformations from TRS calculations are given in Tab. II where the configurations are characterised by parity ( $\pi$ ) and signature ( $\alpha$ ) as  $(\pi, \alpha)$ . The configurations are:  $(+, +1/2)$  (labelled as “A” in the standard nomenclature, defined, for example, in Ref. [47]),  $(+, -1/2)$  (B),  $(-, -1/2)$  (E), and  $(-, +1/2)$  (F). In  $^{111}\text{Xe}$ , the E and F configurations are due to the occupation of  $h_{11/2}$  neutron orbitals and the A and B configurations are due to  $d_{5/2}$  and  $g_{7/2}$  neutron orbitals. In the neighboring odd- $A$  xenon isotopes, the yrast  $\nu h_{11/2}$  bands correspond to the E configuration. The results of the TRS calculations reveal that all of the configurations considered in  $^{111}\text{Xe}$  (E, F, A, and B) have well-developed prolate deformations with  $\beta_2 \simeq 0.170$  for the positive-parity configurations and  $\beta_2 = 0.186$  for the negative-

parity configurations. The  $\gamma$  deformation parameters are small, all being within  $6^\circ$  of zero, suggesting that the configurations are all essentially axially symmetric. Systematic CSM calculations, with input deformation parameters spanning the range of TRS-predicted values, reveal that the resulting quasiparticle diagrams do not vary appreciably with deformation over this range meaning that quasiparticle diagrams calculated at an average deformation are applicable for any of the configurations (A, B, E, F) considered. Thus, average deformation parameters of  $\beta_2 = 0.180$ ,  $\beta_4 = 0.04$ , and  $\gamma = 2^\circ$  were used. The calculations predict that the lowest-frequency quasiparticle alignment is due to a pair of  $h_{11/2}$  neutrons (EF alignment) at a rotational frequency of  $\sim 0.35$  MeV/ $\hbar$ . The next alignment is due to a pair of  $h_{11/2}$  protons (ef alignment) at  $\sim 0.45$  MeV/ $\hbar$ . Pairs of positive-parity neutrons and protons are not predicted to align below  $\sim 0.65$  MeV/ $\hbar$ ; this is beyond the limit of observation for  $^{111}\text{Xe}$  in this work, so the alignment of positive-parity neutrons and protons is not considered further. In the yrast  $\nu h_{11/2}$  bands in the odd- $A$  xenon isotopes, the lowest  $h_{11/2}$  neutron alignment (EF) is blocked by the odd  $h_{11/2}$  neutron, and is therefore not observed. However, the lowest  $h_{11/2}$  proton alignment is not blocked, and should be observed. These expectations are confirmed by experimental data for  $^{113,115,117,119,121}\text{Xe}$  in Refs. [19, 22, 23, 26, 31]. If the band observed here in  $^{111}\text{Xe}$  is the favored signature of the yrast  $\nu h_{11/2}$  band, as suggested by excitation-energy systematics, then the proton  $h_{11/2}$  alignment (ef) should be observed but the neutron  $h_{11/2}$  alignment (EF) will be blocked.

Aligned angular momenta ( $i_x$ ) have been extracted from the experimental data using the method described in Ref. [48]. The  $i_x$  values for  $^{111}\text{Xe}$  are shown in Fig. 4 in comparison to values from neighboring heavier odd- $A$  xenon isotopes [Panel (a)] and even-even xenon isotopes [Panel(b)]. A variable moment-of-inertia reference angular momentum with Harris parameters [49] of  $\mathcal{J}_0=15.0$  MeV $^{-1}\hbar^2$  and  $\mathcal{J}_1=25.0$  MeV $^{-3}\hbar^4$  has been subtracted from all of the data points. These parameters have previously been used for the study of aligned angular momenta in the neutron-deficient xenon isotopes in Refs. [21, 26]. In Fig. 4(a) it can be seen that the data for  $^{115,117,119,121}\text{Xe}$  show a very clear backbend at a rotational frequency of  $\sim 0.45$  MeV/ $\hbar$ . In Refs. [19, 22, 23, 26] this alignment is assigned to be the first  $h_{11/2}$  proton alignment (ef) or the second  $h_{11/2}$  neutron alignment (FG). For  $^{113}\text{Xe}$ , the behavior of the  $i_x$  data is less clear than for the heavier isotopes. The  $i_x$  values have a slight upward curvature between 0.4 and 0.6 MeV/ $\hbar$ , before a downward trend at the highest frequencies. It is difficult to explain the behavior at the highest frequencies although the highest-spin

states in such bands are often tentative.

The data for  $^{111}\text{Xe}$  show a remarkably flat behavior. The aligned angular momentum starts at around  $4\hbar$  and remains constant at this value over the entire range of rotational frequencies observed. For the even-even xenon isotopes shown on Fig. 4(b), the data points for  $^{114}\text{Xe}$  are the most extended in rotational frequency; they clearly show a sharp upbend at a rotational frequency of  $\sim 0.38\text{ MeV}/\hbar$ , followed by a more gradual upbend continuing to the highest observed rotational frequencies. The data for  $^{110,112}\text{Xe}$  are less extended, but have a similar behavior to  $^{114}\text{Xe}$  where data are available. For the even-even  $^{110,112,114}\text{Xe}$  nuclei, neither the first  $h_{11/2}$  neutron (EF) nor the first  $h_{11/2}$  proton alignment (ef) is blocked, and both should be observed. The two distinct regions in the  $i_x$  data for  $^{114}\text{Xe}$  have been assigned to be the  $h_{11/2}$  (EF) neutron alignment, followed by the  $h_{11/2}$  (ef) proton alignment. In comparison, the data for  $^{111}\text{Xe}$  are flat and constant throughout the frequency range where the ef alignment takes place. In  $^{111}\text{Xe}$ , there is no evidence for any increase in aligned angular momentum at the frequency where the proton alignment is observed in  $^{114}\text{Xe}$ .

The flat behavior of the  $i_x$  data for  $^{111}\text{Xe}$  is very interesting. Such behavior could arise as a consequence of the particular variable moment-of-inertia reference that has been subtracted but in this case the same reference has been subtracted and there remains a clear difference in behavior of the  $i_x$  values in  $^{111}\text{Xe}$  compared with the neighboring odd-A  $^{113,115}\text{Xe}$  isotopes. For  $^{111}\text{Xe}$ , there is no sign of a sharp backbend, or even a gradual upbend, that could be attributed to the expected  $h_{11/2}$  proton alignment. However, the shapes of such plots should be studied with caution. When a sharp backbend occurs (low interaction strength), the rotational frequency reduces while  $i_x$  increases giving a characteristic S-shaped plot. When only the first few data points are observed, they form the bottom part of the S shape. With additional data points, the shape can “bend back” revealing a rotational alignment centered at a lower frequency than the maximum frequency of the first few data points. Thus, the lowest few data points can give the misleading impression that an alignment is absent or delayed, when the alignment only becomes apparent with additional data points. Although this is possible for  $^{111}\text{Xe}$ , there is no sign of the onset of a backbend up to a rotational frequency of  $0.5\text{ MeV}/\hbar$ . For the  $^{115,117,119,121}\text{Xe}$  isotopes, there is a very clear backbend at  $\sim 0.45\text{ MeV}/\hbar$ , corresponding to the first  $h_{11/2}$  (ef) proton alignment, but this becomes less clear, and delayed in frequency for  $^{113}\text{Xe}$ . If the delay (in  $^{113}\text{Xe}$ ) is the start of a trend, then it could be that the alignment is delayed still further, to at least  $0.6\text{ MeV}/\hbar$  in  $^{111}\text{Xe}$ .

Although the data in  $^{111}\text{Xe}$  are limited, it is clear that the  $h_{11/2}$  proton alignment is either significantly delayed or absent compared to theoretical predictions and to systematics of the neighboring nuclei. This observation is difficult to explain. However, it is worth noting that for the odd- $A$  xenon isotopes, as the neutron number  $N$  decreases towards  $N = Z$ , the neutrons and protons will occupy increasingly similar orbitals. For  $^{111}\text{Xe}$  with  $N = Z + 3$ , both the neutron and proton Fermi levels are expected to lie in the low- $\Omega$  orbitals of the  $h_{11/2}$  subshells. The alignment of  $h_{11/2}$  protons will therefore take place in the presence of neutrons in near identical orbitals. It is possible that this may give rise to strong neutron-proton correlations which are not taken into account in the CSM calculations performed here. In Ref. [50], calculations suggest that, close to  $N = Z$ , instead of pairs of neutrons or pairs of protons aligning, then neutron-proton pairs may align. For the odd- $A$  nucleus  $^{111}\text{Xe}$ , the odd neutron may block this effect. An alternative explanation is that the delay or absence of the proton alignment is due to the onset of strong octupole correlations between nucleons in the  $h_{11/2}$  and  $d_{5/2}$   $\Delta\ell = \Delta j = 3$  subshells. It was pointed out by Nazarewicz and Olanders in Ref. [51] that strong octupole correlations can lead to the averaging of the quasiparticle alignment; the quasiparticle Routhians calculated with non-zero  $\beta_3$  have a lower gradient than those for the reflection-symmetric case, so any backbend or upbend in the alignment plot would be washed out over a large frequency range, and a clear upbend or backbend would not be observed. Presently, these explanations of the behavior of the proton alignment are speculative. The observations in  $^{111}\text{Xe}$  highlight the need for a better theoretical understanding of the high-spin structure of exotic nuclei in this region.

## VI. SUMMARY

In summary, fifteen  $\gamma$ -ray transitions have been assigned to the decay of excited states in  $^{111}\text{Xe}$ , in an experiment at the Accelerator Laboratory of the University of Jyväskylä. The recoil-decay tagging method was used, with two consecutive  $\alpha$  particles from the  $^{111}\text{Xe} \rightarrow ^{107}\text{Te} \rightarrow ^{103}\text{Sn}$  decay chain providing the required selectivity. A sequence of five  $\gamma$ -ray transitions, identified from recoil-decay tagged  $\gamma\gamma$  coincidences has been assigned as the yrast  $\nu h_{11/2}$  band, on the basis of excitation-energy systematics. The aligned angular momenta in the band have been studied as a function of rotational frequency. In contrast to the neighboring odd- $A$  xenon nuclei there is no evidence for the first  $(h_{11/2})^2$  proton alignment,

despite the theoretical prediction of this alignment at  $0.45 \text{ MeV}/\hbar$ . Indeed, the behavior of the aligned angular momenta in the  $^{111}\text{Xe}$  band is remarkably flat as a function of rotational frequency. The reason for the delay or absence of the first quasiparticle alignment is not clear, though the frequency may be influenced by  $np$  interactions between the aligning  $h_{11/2}$  protons and  $h_{11/2}$  neutrons in similar orbitals, or by the onset of octupole correlations close to  $N = Z = 56$ . It would be of considerable interest to extend the  $\nu(h_{11/2})$  sequence in  $^{111}\text{Xe}$  to identify the frequency of the first quasiparticle alignment.

This work has been supported by the Science and Technology Facilities Council (UK) under grants ST/J000183/2 (UWS) and ST/L005808/1 (UWS). It was also supported by the EU 7th Framework Programme “Integrating Activities - Transnational Access” Project No. 262010 (ENSAR) and by the Academy of Finland under the Finnish Centre of Excellence Programme (Nuclear and Accelerator Based Physics Programme at JYFL; contract 213503). The Authors acknowledge support of Gammapool for the loan of the Jurogam HPGe detectors.

- 
- [1] NuPECC Long Range Plan 2017: Perspectives in Nuclear Physics, [Online]. 2017. <http://www.nupecc.org/pub/lrp17/lrp2017.pdf> [June 2019].
  - [2] P.-H. Heenen, J. Skalski, P. Bonche, and H. Flocard, *Phys. Rev. C* **50**, 802 (1994).
  - [3] J. Skalski, *Phys. Lett. B* **238**, 6 (1990).
  - [4] S. Raman, J. A. Sheikh, and K. H. Bhatt, *Phys. Rev. C* **52**, 1380 (1995).
  - [5] J. F. Smith, C. J. Chiara, D. B. Fossan, D. R. LaFosse, G. J. Lane, J. M. Sears, K. Starosta, M. Devlin, F. Lerma, D. G. Sarantites, S. J. Freeman, M. J. Leddy, J. L. Durell, A. J. Boston, E. S. Paul, A. T. Semple, I. Y. Lee, A. O. Macchiavelli, and P. H. Heenen, *Phys. Lett. B* **523**, 13 (2001).
  - [6] M. Sandzelius, B. Hadinia, B. Cederwall, K. Andgren, E. Ganioglu, I. G. Darby, M. R. Dimmock, S. Eeckhaudt, T. Grahn, P. T. Greenlees, E. Ideguchi, P. M. Jones, D. T. Joss, R. Julin, S. Juutinen, A. Khaplanov, M. Leino, L. Nelson, M. Niikura, M. Nyman, R. D. Page, J. Pakarinen, E. S. Paul, M. Petri, P. Rahkila, J. Saren, C. Scholey, J. Sorri, J. Uusitalo, R. Wadsworth, and R. Wyss *Phys. Rev. Lett.* **99**, 022501 (2007).

- [7] K.-H. Schmidt, R. S. Simon, J.-G. Keller, F. P. Hessberger, G. Munzenberg, B. Quint, H.-G. Clerc, W. Schwab, U. Gollerthan, and C.-C. Sahm, *Phys. Lett. B* **168**, 39 (1986).
- [8] E. S. Paul, P. J. Woods, T. Davinson, R. D. Page, P. J. Sellin, C. W. Beausang, R. M. Clark, R. A. Cunningham, S. A. Forbes, D. B. Fossan, A. Gizon, J. Gizon, K. Hauschild, I. M. Hibbert, A. N. James, D. R. LaFosse, I. Lazarus, H. Schnare, J. Simpson, R. Wadsworth, and M. P. Waring *Phys. Rev. C* **51**, 78 (1995).
- [9] K. Auranen, D. Seweryniak, M. Albers, A. D. Ayangeakaa, S. Bottoni, M. P. Carpenter, C. J. Chiara, P. Copp, H. M. David, D. T. Doherty, J. Harker, C. R. Hoffman, R. V. F. Janssens, T. L. Khoo, S. A. Kuvin, T. Lauritsen, G. Lotay, A. M. Rogers, J. Sethi, C. Scholey, R. Talwar, W. B. Walters, P. J. Woods, and S. Zhu. *Phys. Rev. Lett.* **121**, 182501 (2018).
- [10] D. Schardt, R. Kirchner, O. Klepper, W. Reisdorf, E. Roeckl, P. Tidemand-Petersson, G. T. Ewan, E. Hagberg, B. Jonson, S. Mattsson, and G. Nyman, *Nucl. Phys.* **A326**, 65 (1979).
- [11] R. D. Page, P. J. Woods, R. A. Cunningham, T. Davinson, N. J. Davis, A. N. James, K. Livingston, P. J. Sellin, and A. C. Shotter, *Phys. Rev. C* **49**, 3312 (1994).
- [12] L. Cartegni, C. Mazzocchi, R. Grzywacz, I. G. Darby, S. N. Liddick, K. P. Rykaczewski, J. C. Batchelder, L. Bianco, C. R. Bingham, E. Freeman, C. Goodin, C. J. Gross, A. Guglielmetti, D. T. Joss, S. H. Liu, M. Mazzocco, S. Padgett, R. D. Page, M. M. Rajabali, M. Romoli, P. J. Sapple, J. Thomson, and H. V. Watkins, *Phys. Rev. C* **85**, 014312 (2012).
- [13] C. Mazzocchi, Z. Janas, L. Batist, V. Belleguic, J. Doring, M. Gierlik, M. Kapica, R. Kirchner, G. A. Lalazissis, H. Mahmud, E. Roeckl, P. Ring, K. Schmidt, P. J. Woods, and J. Zylicz, *Phys. Lett. B* **532**, 29 (2002).
- [14] S. N. Liddick, R. Grzywacz, C. Mazzocchi, R. D. Page, K. P. Rykaczewski, J. C. Batchelder, C. R. Bingham, I. G. Darby, G. Drafta, C. Goodin, C. J. Gross, J. H. Hamilton, A. A. Hecht, J. K. Hwang, S. Ilyushkin, D. T. Joss, A. Korgul, W. Królas, K. Lagergren, K. Li, M. N. Tantawy, J. Thomson, and J. A. Winger *Phys. Rev. Lett.* **97**, 082501 (2006).
- [15] I. G. Darby, R. K. Grzywacz, J. C. Batchelder, C. R. Bingham, L. Cartegni, C. J. Gross, M. Hjorth-Jensen, D. T. Joss, S. N. Liddick, W. Nazarewicz, S. Padgett, R. D. Page, T. Papenbrock, M. M. Rajabali, J. Rotureau, and K. P. Rykaczewski, *Phys. Rev. Lett.* **105**, 162502 (2010).



- [16] D. Schardt, T. Batsch, R. Kirchner, O. Klepper, W. Kurcewicz, E. Roeckl, and P. Tidemand-Petersson, Nucl. Phys. **A368**, 153 (1981).
- [17] F. Heine, T. Faestermann, A. Gillitzer, J. Homolka, M. Kopf, and W. Wagner, Z. Phys. A **340**, 225 (1991).
- [18] M. Serris, C. T. Papadopoulos, R. Vlastou, C. A. Kalfas, S. Kossionides, N. Fotiades, S. Harisopulos, C. W. Beausang, M. J. Joyce, E. S. Paul, M. A. Bentley, S. Araddad, J. Simpson, and J. F. Sharpey-Schafer, Z. Phys. A **358**, 37 (1997).
- [19] J. Timár, J. Simpson, E. S. Paul, S. Araddad, C. W. Beausang, M. A. Bentley, M. J. Joyce, J. F. Sharpey-Schafer, J. Phys. G: Nucl. Part. Phys. **21**, 783 (1995).
- [20] C.-B. Moon, T. Komatsubara, T. Shizuma, K. Uchiyama, Y. Sasaki, and K. Furuno, Eur. Phys. J. A **4**, 107 (1999).
- [21] S. Törmänen, S. Juutinen, R. Julin, B. Cederwall, A. Johnson, R. Wyss, P. Ahonen, B. Fant, M. Matsuzaki, J. Nyberg, M. Piiparinen, S. Mitarai, J. Mukai, and A. Virtanen, Nucl. Phys. **A572**, 417 (1994).
- [22] H. C. Scraggs, E. S. Paul, A. J. Boston, J. F. C. Cocks, D. M. Cullen, K. Helariutta, P. M. Jones, R. Julin, S. Juutinen, H. Kankaanpää, M. Muikku, P. J. Nolan, C. M. Parry, A. Savelius, R. Wadsworth, A. V. Afanasjev, and I. Ragnarsson, Nucl. Phys. **A640**, 337 (1998).
- [23] E. S. Paul, H. C. Scraggs, A. J. Boston, D. B. Fossan, K. Hauschild, I. M. Hibbert, P. J. Nolan, H. Schnare, J. M. Sears, I. Thorslund, R. Wadsworth, A. N. Wilson, and J. N. Wilson, Nucl. Phys. **A644**, 3 (1998).
- [24] J. M. Sears, D. B. Fossan, G. R. Gluckman, J. F. Smith, I. Thorslund, E. S. Paul, I. M. Hibbert, R. Wadsworth, Phys. Rev. C **57**, 2991 (1998).
- [25] G. de Angelis, A. Gadea, E. Farnea, R. Isocrate, P. Petkov, N. Marginean, D. R. Napoli, A. Dewald, M. Bellato, A. Bracco, F. Camera, D. Curien, M. De Poli, E. Fioretto, A. Fitzler, S. Kasemann, N. Kintz, T. Klug, S. Lenzi, S. Lunardi, R. Menegazzo, P. Pavan, J. L. Pedroza, V. Pucknell, C. Ring, J. Sampson, and R. Wyss, Phys. Lett. B **535**, 93 (2002).
- [26] E. S. Paul, H. R. Andrews, T. E. Drake, J. DeGraaf, V. P. Janzen, S. Pilotte, D. C. Radford, and D. Ward, Phys. Rev. C **53**, 2520 (1996).
- [27] E. S. Paul, H. C. Scraggs, A. J. Boston, O. Dorvaux, P. T. Greenlees, K. Helariutta, P. Jones, R. Julin, S. Juutinen, H. Kankaanpää, H. Kettunen, M. Muikku, P. Nieminen, P. Rahkila,

- and O. Stezowski, Nucl. Phys. **A673**, 31 (2000).
- [28] E. S. Paul, A. J. Boston, H. J. Chantler, P. J. Nolan, M. P. Carpenter, R. V. F. Janssens, F. G. Kondev, D. Seweryniak, C. J. Chiara, D. B. Fossan, T. Koike, K. Starosta, A. M. Fletcher, J. C. Lisle, D. Patel, J. F. Smith, D. R. LaFosse, W. Reviol, D. G. Sarantites, R. Wadsworth, A. N. Wilson, and I. Ragnarsson Phys. Rev. C **65**, 051308(R) (2002).
  - [29] D. G. Sarantites, P.-F. Hua, M. Devlin, L. G. Sobotka, J. Elson, J. T. Hood, D. R. LaFosse, J. E. Sarantites, and M. R. Maier, Nucl. Instrum. Methods Phys. Res. A **381**, 418 (1996).
  - [30] D. G. Sarantites, W. Reviol, C. J. Chiara, R. J. Charity, L. G. Sobotka, M. Devlin, M. Furlotti, O. L. Pechenaya, J. Elson, P. Hausladen, S. Fischer, D. Balamuth, and R. M. Clark, Nucl. Instrum. Methods Phys. Res. A **530**, 473 (2004).
  - [31] H. C. Scraggs, E. S. Paul, A. J. Boston, C. J. Chiara, M. Devlin, O. Dorvaux, D. B. Fossan, P. T. Greenlees, K. Helariutta, P. Jones, R. Julin, S. Juutinen, H. Kankaanpää, H. Kettunen, D. R. LaFosse, G. J. Lane, I. Y. Lee, A. O. Macchiavelli, M. Muikku, P. Nieminen, P. Rahkila, D. G. Sarantites, J. M. Sears, A. T. Semple, J. F. Smith, K. Starosta, and O. Stezowski, Phys. Rev. C **61**, 064316 (2000).
  - [32] P. J. Nolan, Nucl. Phys. **A520**, 657c (1990).
  - [33] M. Leino, J. Äystö, T. Enqvist, P. Heikkinen, A. Jokinen, M. Nurmi, A. Ostrowski, W. H. Trzaska, J. Uusitalo, K. Eskola, P. Armbruster, and V. Ninov Nucl. Instrum. Methods Phys. Res., Sect B **99** (1995) 653.
  - [34] R. D. Page, A. N. Andreyev, D. E. Appelbe, P. A. Butler, S. J. Freeman, P. T. Greenlees, R.-D. Herzberg, D. G. Jenkins, G. D. Jones, P. Jones, D. T. Joss, R. Julin, H. Kettunen, M. Leino, P. Rahkila, P. H. Regan, J. Simpson, J. Uusitalo, S. M. Vincent, R. Wadsworth Nucl. Instrum. Methods Phys. Res., Sect B **204**, 138 (2003).
  - [35] I. H. Lazarus, D. E. Appelbe, P. A. Butler, P. J. Coleman-Smith, J. R. Cresswell, S. J. Freeman, R. D. Herzberg, I. Hibbert, D. T. Joss, S. C. Letts, R. D. Page, V. F. E. Pucknell, P. H. Regan, J. Sampson, J. Simpson, J. Thornhill, and R. Wadsworth, IEEE Trans. Nucl. Sci. **48** 567 (2001).
  - [36] L. Capponi, Ph.D. thesis, University of the West of Scotland (2014).
  - [37] P. Rahkila, Nucl. Instrum. Methods Phys. Res., Sect A **595**, 637 (2008).
  - [38] D. C. Radford, Nucl. Inst. Methods Phys. Res., Sect. A **361**, 297 (1995).
  - [39] D. C. Radford, Nucl. Inst. Methods Phys. Res., Sect. A **361**, 306 (1995).

- [40] L. Capponi, J. F. Smith, P. Ruotsalainen, C. Scholey, P. Rahkila, B. Hadinia, L. Bianco, A. J. Boston, H. C. Boston, D. M. Cullen, X. Derkx, M. Drummond, T. Grahm, P. T. Greenlees, L. Grocutt, U. Jakobsson, D. T. Joss, R. Julin, S. Juutinen, M. Labiche, M. Leino, K. Leach, C. McPeake, K. F. Mulholland, P. Nieminen, D. O'Donnell, E. S. Paul, P. Peura, M. Sandzelius, J. Saren, B. Saygi, J. Sorri, A. Thornthwaite, M. J. Taylor, and J. Uusitalo, to be submitted.
- [41] E. S. Paul, A. J. Boston, S. Courtin, P. J. Dagnall, J. L. Durell, C. Finck, B. Gall, B. Haas, F. Haas, F. Hannachi, F. Hoellinger, J. C. Lisle, A. Lopez-Martens, J. C. Merdinger, N. Rowley, H. C. Scraggs, O. Stezowski, B. J. Varley, and J. P. Vivien, *Eur. Phys. J. A* **7**, 449 (2000).
- [42] P. Moller, J. R. Nix, W. D. Myers, and W. J. Swiatecki, *At. Data Nucl. Data Tables* **59**, 185 (1995).
- [43] F. Nowacki *et al.*, private communication (2015).
- [44] R. Wyss, J. Nyberg, A. Johnson, R. Bengtsson, and W. Nazarewicz, *Phys. Lett. B* **215**, 211 (1988).
- [45] W. Nazarewicz, R. Wyss, and A. Johnson, *Nucl. Phys.* **A503**, 285 (1989).
- [46] W. Nazarewicz, J. Dudek, R. Bengtsson, T. Bengtsson, and I. Ragnarsson, *Nucl. Phys.* **A435** 397 (1985).
- [47] R. Wyss *et al.*, *Nucl. Phys.* **A503**, 244 (1989).
- [48] R. Bengtsson and S. Frauendorf, *Nucl. Phys.* **A327**, 139 (1979).
- [49] S. M. Harris, *Phys. Rev. B* **138**, 509 (1965).
- [50] E. Caurier, F. Nowacki, A. Poves and K. Sieja, *Phys. Rev. C* **82**, 064304 (2010).
- [51] W. Nazarewicz and P. Olanders, *Nucl. Phys.* **A441**, 420 (1985).

TABLE I: Properties of  $\gamma$ -ray transitions assigned to  $^{111}\text{Xe}$ . The relative intensities ( $I_\gamma$ ) are corrected for detection efficiency and are normalised to the intensity of 405-keV transition. The initial and final spins and parities ( $I_i^{\pi_i}$  and  $I_f^{\pi_f}$ ), where given in the right-hand column, are tentatively assigned from systematics.

$E_\gamma$ (keV)	$I_\gamma$	$I_i^{\pi_i} \rightarrow I_f^{\pi_f}$
114.8(7)	13(5)	
125.5(8)	10(5)	
381.6(9)	24(10)	
405.3(3)	100(16)	(15/2 <sup>-</sup> ) $\rightarrow$ (11/2 <sup>-</sup> )
434.6(5)	30(9)	
490.5(4)	67(12)	
532.9(5)	56(13)	
560.2(8)	22(9)	
618.9(8)	48(17)	(19/2 <sup>-</sup> ) $\rightarrow$ (15/2 <sup>-</sup> )
676.1(9)	30(18)	
759.9(5)	30(14)	
782.7(5)	42(14)	(23/2 <sup>-</sup> ) $\rightarrow$ (19/2 <sup>-</sup> )
920(1)	20(10)	(27/2 <sup>-</sup> ) $\rightarrow$ (23/2 <sup>-</sup> )
1028.0(14)	13(10)	
1048 (1)	12(10)	(31/2 <sup>-</sup> ) $\rightarrow$ (27/2 <sup>-</sup> )

TABLE II: Deformations of configurations of the odd neutron in  $^{111}\text{Xe}$ , from Total Routhian Surface (TRS) calculations. The left-hand column gives the orbital of the neutron in the standard nomenclature. The other three columns give the  $\beta_2$ ,  $\gamma$ , and  $\beta_4$  deformation parameters calculated at a rotational frequency of  $\omega \simeq 0.195 \text{ MeV}/\hbar$ . This frequency is chosen because it is just below the first quasiparticle alignment in the neighboring even-even nuclei.

$\nu(\pi, \alpha)$	$\beta_2$	$\gamma(^{\circ})$	$\beta_4$
A(+, +1/2)	0.173	-4.7	0.039
B(+, -1/2)	0.170	-3.3	0.034
E(-, -1/2)	0.186	+5.8	0.043
F(-, +1/2)	0.186	-2.3	0.043

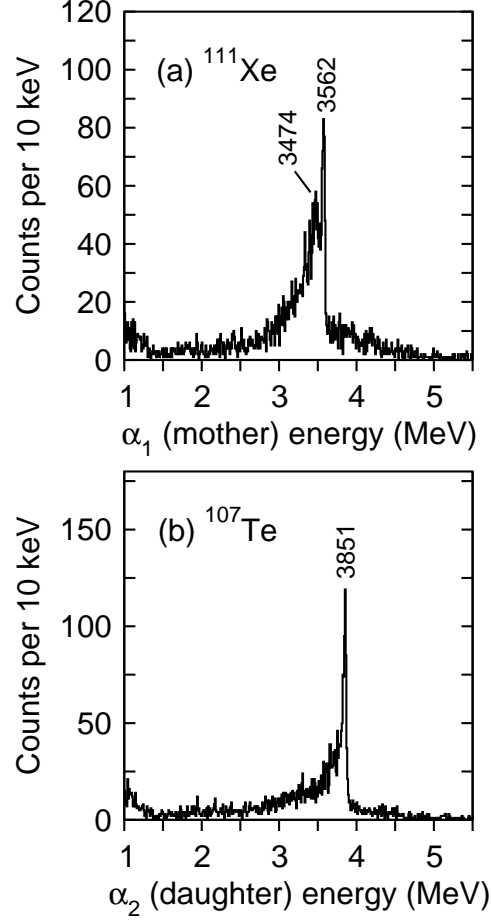


FIG. 1: Projections of the  $\alpha\alpha$  correlation matrix, incremented by the energies of two successive  $\alpha$  decays following an implant in the DSSD, as described in the text. The matrix is incremented if the time difference between the implant and first  $\alpha$  decay is less than 6 s, and that between the first and second  $\alpha$  decays is less than 12 ms. Panel (a) shows the  $\alpha$ -particle energy of the first  $\alpha$  decay, corresponding to  $^{111}\text{Xe}$ , and panel (b) shows the  $\alpha$ -particle energy of the second  $\alpha$  decay, corresponding to  $^{107}\text{Te}$ .

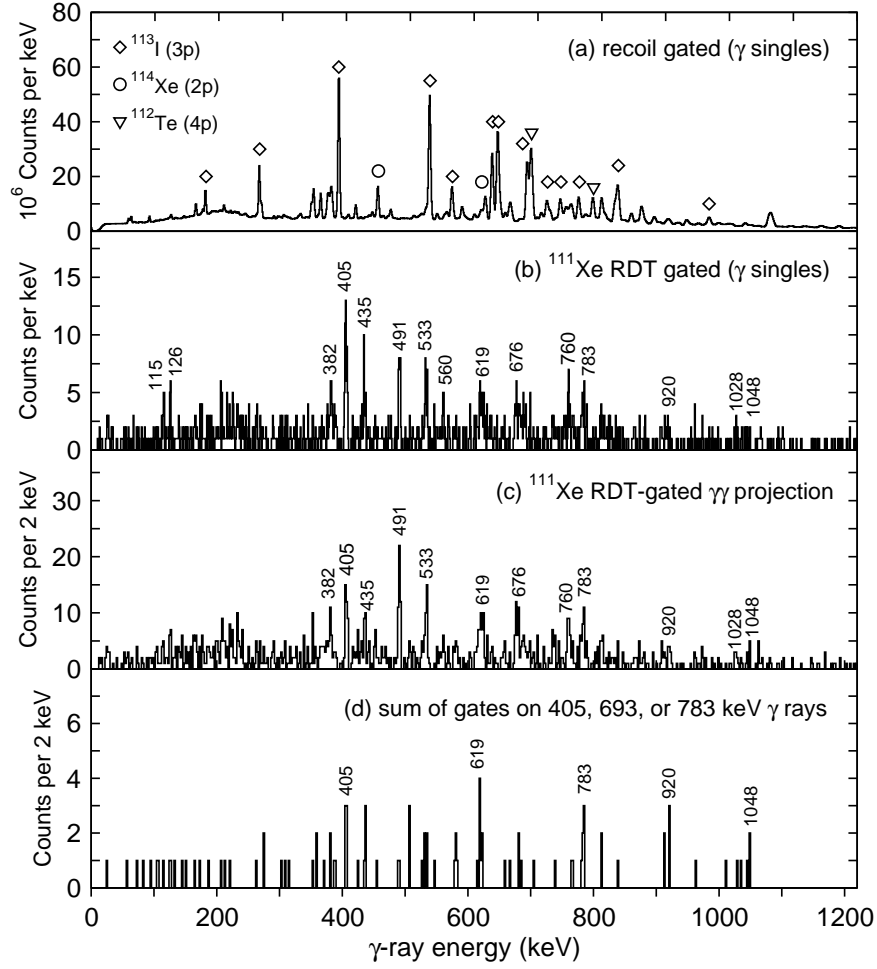


FIG. 2: Representative  $\gamma$ -ray spectra from the  $^{58}\text{Ni} + ^{58}\text{Ni}$  reaction, collected with the Jurogam-II  $\gamma$ -ray spectrometer. Panel (a) shows energies of all of the  $\gamma$  rays collected in the period between 80 and 400 ns before the detection of an implanted evaporation residue in the DSSDs. The spectra in panels (b), (c), and (d) have been incremented with the implant- $\alpha(^{111}\text{Xe})$ - $\alpha(^{107}\text{Te})$  RDT condition, as described in the text. Panel (b) shows all of the  $\gamma$  rays. Panel (c) shows the projection of a symmetrized  $\gamma\gamma$  correlation matrix. It should be noted that the spectra in Panels (c) and (d) have a dispersion of 2 keV per channel, whereas the spectra in Panels (a) and (b) have a dispersion of 1 keV per channel. Panel (d) shows a sum of gates on some of the strongest transitions in the  $\gamma\gamma$  matrix; specifically - 405-, 619-, or 783-keV transitions. All of the peaks that are labelled on Panels (b), (c), and (d) correspond to  $\gamma$ -ray transitions that have been assigned to  $^{111}\text{Xe}$ .

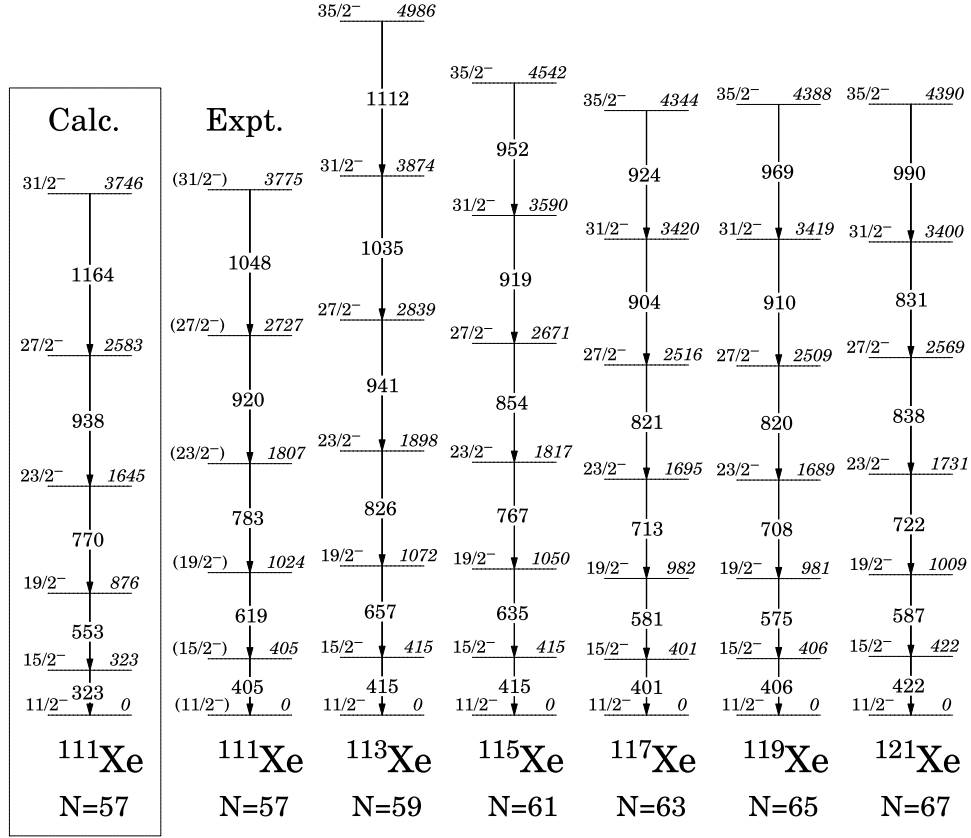


FIG. 3: Excitation energies of states in the yrast  $\nu h_{11/2}$  bands in the odd- $A$  xenon isotopes up to spin  $35/2^-$ , relative to the excitation energies of the  $11/2^-$  band heads. The data for  $^{113,115,117,119,121}\text{Xe}$  are taken from Refs. [19, 22, 23, 26, 31]. For  $^{111}\text{Xe}$ , the data marked “Expt” and “Calc” show the experimental and calculated data, respectively. The experimental data for  $^{111}\text{Xe}$  are derived from the experimental work presented here, and the calculated data are from shell-model calculations [43].



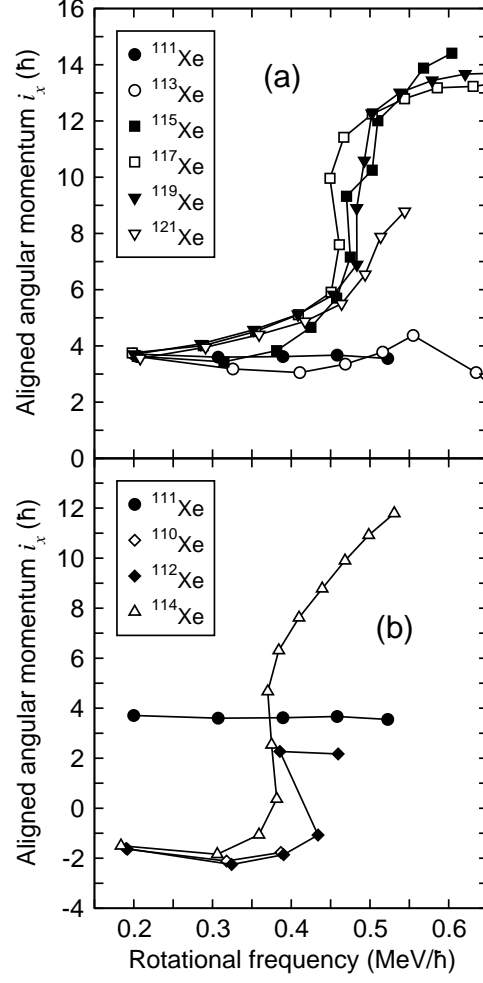


FIG. 4: Aligned angular momenta of states in the yrast bands of neutron-deficient xenon isotopes. Panel (a) shows data for the  $^{111}\text{Xe}$  band compared to that of the yrast  $\nu h_{11/2}$  bands of odd- $A$  xenon isotopes with  $113 \leq A \leq 121$ . Panel (b) shows the  $^{111}\text{Xe}$  data compared to that of the ground-state bands of  $^{110,112,114}\text{Xe}$ . For all data points a reference configuration with Harris parameters [49] of  $\mathcal{J}_0=15.0 \text{ MeV}^{-1}\hbar^2$  and  $\mathcal{J}_1=25.0 \text{ MeV}^{-3}\hbar^4$  has been subtracted. The data for  $^{110,112,113,114,115,117,119,121}\text{Xe}$  are derived from level schemes presented in Refs. [5, 6, 19, 22, 23, 26, 27, 31]. The data for  $^{111}\text{Xe}$  are taken from the present work.